

Chapter 2

The Turbulence Damping Effect on the Slug Flow Modeling



Harley Henrique Parno, Bruna Iten Bittelbrunn, Carla Nayara Michels dos Santos, Sarah Laysa Becker, Christine Fredel Boos, Celso Murilo dos Santos, Waldir Pedro Martignoni, and Henry França Meier

Abstract The slug flow is one of the most complex flow patterns due to the unstable behavior of phase distribution. This pattern occurs in a wide range of flow rates and therefore is observed in different industrial processes. The prediction and understanding of the hydrodynamic parameters of this flow regime have a significant engineering value. In this context, Computational Fluid Dynamics (CFD) has been shown to be an efficient tool for the prediction of this type of flow. However, to ensure the accuracy of the numerical solution, adequate modeling of interfacial properties transfer is necessary. One of the most important interface transfer phenomena is momentum transfer between phases. Therefore, it is necessary to use a robust approach to model the gas–liquid interface region. The aim of this study is to evaluate the effect of adding the damping of turbulent diffusion at the interface on flow modeling. For this, different cases of simulations were elaborated for a pipe with 2 m in length and 26 mm inner diameter. In all the cases, the multiphase approach used was the Volume of Fluid (VOF) with the Geo-Reconstruct scheme. The interface between the fluids was modeled with constant surface tension equal to 0.0728 N/m. The discontinuities present at the interface were treated in a “continuous surface stress” (CSS) manner. The turbulence was modeled using $k\omega$ -SST with and without turbulence damping. The independence of the numerical solution in relation to the grid was evaluated by the Grid Convergence Index (GCI) method in which four levels of grid were used. Preliminary results showed that, in the cases with turbulence damping, a better representation of the flow pattern morphology was obtained. Regarding the quantitative parameters, the prominent frequency of the Power Spectral Density (PSD) of the pressure signal was under-predicted when the turbulence damping was not used.

H. H. Parno · B. I. Bittelbrunn · C. N. M. dos Santos · S. L. Becker · C. F. Boos · C. M. dos Santos · W. P. Martignoni · H. F. Meier (✉)
University of Blumenau, 3250 São Paulo Street, Blumenau, SC, Brazil
e-mail: meier@furb.br

H. H. Parno
e-mail: hparno@furb.br

C. F. Boos
e-mail: cfboos@furb.br

Keywords Slug flow · Interfacial modeling · Turbulence damping

2.1 Introduction

Two-phase flows are observed in numerous industrial and natural processes. Due to the surface tension force, an interface between the fluids is created and the fluids flow separately such as bubbles and droplets. Additionally, the gravity force segregates the flow by differences in density. As a result, horizontal two-phase flow is naturally stratified. However, the difference in fluid density also induces velocity and pressure gradients between phases. The instabilities generated by the gradients develop very small waves. Depending on operating conditions, the mass and momentum transfer between interfacial microwaves develop two-phase flow patterns.

Regarding the gas–liquid flow patterns, intermittent flow is one of the most observed in industrial processes. The slug and plug flows are characterized by a wave that closes the pipe cross-sectional area. The difference between plug and slug flows is the presence of gas bubbles in the liquid slug. Based on the gas quantity inside the liquid slug, the flow is subclassified in low- and high-aerated slugs. Slug flow is characterized by the occurrence of high pressure, velocity, and volume fraction oscillations. High slug frequency not only increases the pressure loss (drop) but also increases the material injury. Because of that, slug flow is undesirable in the majority part of industrial processes such as boilers, refrigeration systems, and several processes in the gas–oil industry. An exception is the two-phase flow in multi-channel reactors, in which some authors related that the slug flow pattern increases the liquid–gas mixture in the reactor channels and the efficiency consequently also increased (Tonomura et al. 2018).

In the last century, several experimental studies have been conducted in order to understand the onset and development of the slug flow, mainly with flow studied in pipelines. Experimental studies commonly use volume fraction and pressure measurements to identify and classify the flow pattern. In addition, a flow visualization study helps to identify the pattern. Besides that, researchers developed charts to predict the gas–liquid flow patterns transition based on both phase-operating conditions (Baker 1953). One of the first explanations for slug formation was conducted by Taitel and Dukler (1976). They explain the formation of slug flow patterns due to the Kelvin–Helmholtz (KH) instabilities. Classical KH instabilities provide stability criteria of infinitesimal amplitude waves to be formed at the free surface.

Several authors have been conducted to propose empirical correlations to predict important parameters in two-phase flow such as frequency. This is one of the most important parameters due to the direct impact on pressure loss and material damage in industrial devices caused by the passage of slugs in the pipes. Empirical correlations based on non-dimensional numbers, such as the Strouhal and Froude numbers, were developed to predict the slug frequency. Gregory and Scott (1969) were the first authors to calculate the slug frequency based on non-dimensional slug frequency. Fossa et al. (2003) were the first author to propose an empirical correlation for slug

frequency based on the Strouhal number. They proposed that the Strouhal number for slug flow is dominated by the gas velocity. Wang et al. (2007) modified the Strouhal number correlation considering the liquid velocity as well.

Recently, an empirical correlation for slug frequency was proposed by Thaker and Banerjee (2015). They assumed that the non-dimensional frequency is a product of Strouhal and Froude numbers. The non-dimensional frequency is obtained by an empirical correlation based on gas and liquid Reynolds numbers and the non-dimensional length. The empirical coefficients were obtained by linear regression of experimental measurements. The experiments were conducted in a wide range of Reynolds numbers for both phases (1400–18,500 for water and 390–7500 for air). The experimental data were obtained in a 25.4 mm pipe diameter and 8 m pipe length. The authors relate that the correlations prediction is in accordance with experimental observations such as the frequency decrease with the length.

Other experimental investigations were carried out in order to develop models to predict other important properties of slug flow, such as slug length, liquid holdup, pressure drop, velocity, and others (Barnea and Brauner 1985; Barnea and Taitel 1993; Cook and Behnia 2000; Gregory and Scott 1969; Greskovich and Shrier 1971; Nydal et al. 1992; Scott et al. 1989; Van Hout et al. 2002). Over time, several numerical strategies have been developed to predict the behavior of this flow pattern in a more detailed way.

For a better understanding of the phenomenon, computational fluid dynamics (CFD) have been used for decades to be able to predict the behavior of this type of flow. Although the one-dimensional (1D) numerical models are capable to predict pressure loss, they are not capable to predict the two-phase flow patterns. However interesting results are reported when a two-dimensional (2D) model is applied. One of the first studies involving two-phase flow 2D interfacial modeling was conducted by Lun et al. (1996). The researchers found a high dependence between numerical results and mesh quality. They showed that a very coarse mesh results in numerical oscillations called wiggles. Wiggles can result in false pressure and volume fraction oscillations and can be wrongly interpreted as a slug flow pattern. On the other hand, when the finest and high-quality mesh was applied, the wave flow pattern was predicted for equal operational conditions.

Regarding the tridimensional (3D) two-phase flow modeling, Vallée et al. (2008) conducted experimental and numerical experiments of gas–liquid flow in a horizontal channel with a rectangular cross section. Optical techniques were applied to measure the dynamic pressure and the results were synchronized with a high-speed camera system. The Euler–Euler two-phase model was applied using the ANSYS CFX code. The turbulence was modeled for each phase separately using the $k-\omega$ SST model, but turbulence damping was not considered. The numerical results showed a good qualitative agreement between experimental and numerical data. On the other hand, the slug flow was generated based on a variable liquid holdup for the inlet boundary condition, equal to the experimental measurements.

Self-generated slugs were modeled by Bartosiewicz et al. (2010). The 3D numerical simulations were carried out with different mathematical modeling and validated

with experimental data. The first experimental slug generated was observed at 0.3–0.7 s and the onset of slug was at 1.5 m. The VOF approach was simulated with laminar, k - ϵ , k - ω , and k - ω SST, and the slug generation was not observed. The two-fluid model was applied with k - ω and a special turbulence damping function at the interface and a slug was obtained after 16.65 s at 3.5 m from the inlet. In addition, a 2D simulation was conducted using the multi-fluid VOF method and k - ϵ turbulence model with a Large Interface Model (LIM) for modeling the momentum transfer through the interface and the slug flow was initiated earlier at 1.6 s and 1.5 m from inlet. On the other hand, Shirodkar (2015) performed a 2D slug flow modeling using the multi-fluid VOF method, symmetric drag law, and k - ω with turbulence damping. It was reported as a reasonable match with the available experimental data in the literature, modeling the first slug at 0.87 s and 1.7 m from inlet.

Friedemann et al. (2019) conducted gas–liquid slug flow validation study in a concentric annulus geometry. Periodic boundary conditions were applied to alleviate the computational requirement. The VOF model was applied with a compressive method to reduce the numerical diffusion at the interface. The k - ω RANS model was used to solve the turbulence and no damping method was mentioned. The researchers concluded that the solution had a strong dependence on the mesh density and domain length.

Akhlaghi et al. (2019) conducted numerical simulations of the plug and slug flows regimes solving the VOF and multi-fluid VOF models. The k - ω SST model was applied to solve the turbulence, but no turbulence damping model was mentioned. The researchers reported that the multi-fluid VOF model provided a larger agreement with experimental data in comparison to the VOF model. On the other hand, the computational time requirement was increased 14 times.

Although a very fine mesh is recommendable to correctly simulate the two-phase interface, they are impracticable for industrial applications. Due to the high computational time requirement, industrial applications are normally conducted in coarse meshes. Because of that, the RANS turbulence models are applied, but additional equations are needed to model the turbulence near the interface. In a recent work, Frederix et al. (2018) presents the Egorov approach. The Egorov approach is a traditional method to model the turbulence damping. On the other hand, a high mesh dependence has been reported and Frederix et al. (2018) modified the turbulence damping model to be mesh independent and extended to the k - ϵ turbulence model. In addition, Höhne and Porombka (2018) improved the turbulence modeling by introducing a model for sub-grid size waves induced by Kelvin–Helmholtz instabilities.

The purpose of the present work is to simulate the turbulent two-phase flow in a high-aerated slug pattern in a horizontal pipe. This also involves a comparison between results with and without an additional equation to damp the turbulent at the gas–liquid interface. In addition, discretization errors were estimated, and numerical data was validated against experimental data available in the literature.

2.2 Mathematical Modeling

In the numerical studies carried out in this research, the fluids were assumed to be immiscible, and without phase change. The VOF (Hirt and Nichols 1981) approach is a classical method used to solve stratified flows. The VOF method tracks the interface between fluids by the solution of Eq. (1), which is the continuity equation for the volume fraction of one of the phases.

$$\frac{\partial}{\partial t}(\alpha_q \rho_q) + \mathbf{v} \cdot \nabla \alpha_q \rho_q = 0, \quad (1)$$

where α_q and ρ_q are the volumetric fraction and density for phase q , respectively, t is the time, and \mathbf{v} is the average velocity vector.

In classical VOF, a single momentum equation is solved, Eq. (2), and the two fluids share the same transport equation. Recently, researchers have been using a multi-fluid VOF (Cerne et al. 2001) method to solve dispersed flows, but the authors emphasized the needed additional computational efforts.

$$\frac{\partial}{\partial t}(\rho \mathbf{v}) + \nabla \cdot (\rho \mathbf{v} \mathbf{v}) = -\nabla P + \nabla \cdot [(\mu + \mu_T)(\nabla \mathbf{v} + \nabla \mathbf{v}^T)] + \rho \mathbf{g} + \mathbf{F}, \quad (2)$$

where μ is the fluid viscosity, μ_T is the turbulent viscosity, P is the average static pressure, \mathbf{F} is the surface tension, and ρ is density.

The fluid properties (density and viscosity, for example) were calculated by Eq. (3).

$$\phi = \sum \alpha_q \phi_q, \quad (3)$$

where ϕ is a general mixture property.

Although density was treated as a constant, gas phase was assumed to be an ideal fluid. Thus, the energy transport equation, Eq. (4), must be solved.

$$\frac{\partial}{\partial t}(\rho E) + \nabla \cdot [\mathbf{v}(\rho E + p)] = \nabla \cdot (k_{\text{eff}} \nabla T), \quad (4)$$

where E stands for energy, which was calculated by Eq. (5), T is the temperature, and k_{eff} is the effective thermal conductivity.

$$E = \frac{\sum_{q=1}^n \alpha_q \rho_q E_q}{\sum_{q=1}^n \alpha_q \rho_q}, \quad (5)$$

where E_q is based on the specific heat of each phase and the shared temperature.

The turbulent viscosity was calculated by Eq. (6), using the two-equation model k - ω SST (Menter 1994).

$$\mu_T = \frac{\rho a_1 k}{\text{Max}(a_1 \omega; S F_2)}, \quad (6)$$

where k is the turbulent kinetic energy, which was calculated by Eq. (7), ω is the specific turbulence dissipation rate which was calculated by Eq. (8), F_2 is a weighting function that is one for boundary-layer flows and zero for free shear layers, S is the strain rate magnitude, and a_1 is a constant.

$$\frac{\partial}{\partial t}(\rho k) + \nabla \cdot (\rho \mathbf{v}k) = \nabla \cdot (\Gamma_k \nabla k) + G_k - Y_k, \quad (7)$$

where Γ_k is the effective diffusivity of k , G_k is the production of k , and Y_k is the dissipation of k due to turbulence.

$$\frac{\partial}{\partial t}(\rho \omega) + \nabla \cdot (\rho \mathbf{v}\omega) = \nabla \cdot (\Gamma_\omega \nabla \omega) + G_\omega - Y_\omega + D_\omega + S_\omega, \quad (8)$$

where Γ_ω is the effective diffusivity of ω , G_ω is the production of ω , Y_ω is the dissipation of ω due turbulence, D_ω is the cross-diffusion term, and S_ω is a source term.

Although this model has a good agreement for near and distant from the wall turbulence, an additional problem is observed in two-phase flow: the gas velocity near the interface reduces and a near-wall compartment was observed. Thus, a damping model was used to correctly compute the turbulence quantities at the interface region. The Egorov approach included the damping turbulence as a source term (S_ω) in the ω equation, calculated by Eq. (9)

$$S_\omega = A \Delta n \beta \rho \left(\frac{6B\mu}{\beta \rho \Delta n^2} \right)^2, \quad (9)$$

where A is the interfacial area, which was calculated by Eq. (10), Δn is the cell height normal to interface, β is a k - ω coefficient, and B is the damping factor

$$A = 2\alpha_q |\nabla \alpha_q|. \quad (10)$$

Additional models were necessary to solve the cells containing the interface. The Geo Reconstruct method, a piece-linear model, was used to solve the numerical diffusion and reconstruct the interface. The surface tension term was modeled in a continuous surface stress (CSS) manner instead of the continuous surface force (CSF), as described by Gueyffier et al. (1999).

2.3 Methods

The computational domain consisted of a pipe with an inner diameter of 26 mm and 2 m in length. Varying mesh densities were generated to evaluate the effect of the mesh resolution and quality on the numerical solution. Firstly, the cross section of pipe was divided into 320 face elements and the longitudinal divisions varied between 60 and 480, allowing to assess the impact of the aspect ratio on the solution. Based on mesh 04, coarse, fine, and extra fine meshes were generated varying all the tridimensional divisions with a constant ratio of approximately 1.3. Additionally, a special attention was paid to the first wall element length in order to solve the turbulence near the wall. A comparison between meshes is presented in Fig. 1 and the mesh information is summarized in Table 1.

The boundary conditions were set as no-slip at the wall and zero pressure at the outlet. The inlet face was horizontally divided into two equal, where air enters the upper part and water in the lower part. The superficial velocities were applied as boundary conditions at the entrance resulting in 9 m/s for air and 0.8 m/s for water phase. The simulation was initialized with a fully developed airflow. The time step was set as a variable with the maximum Courant number equal to 2 and the flow was simulated for 20 s, which was considered sufficient to observe a significant number of slugs. However, the first 2 s, correspondent to 4.9 residence times, were discarded to

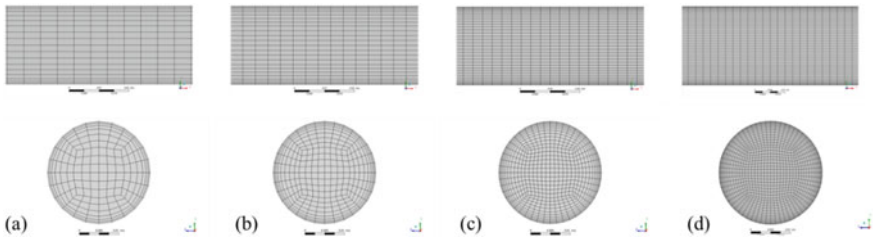


Fig. 1 Mesh. **a** Coarse mesh (mesh 05); **b** intermediate mesh (mesh 04); fine mesh (mesh 06); extra fine mesh (mesh 07)

Table 1 Mesh information

Mesh	Face elements	Longitudinal divisions	Total elements	First wall element
01	320	60	18,880	0.00020
02	320	120	38,080	0.00020
03	320	240	76,480	0.00020
04	320	480	153,280	0.00020
05	180	360	64,620	0.00030
06	672	625	419,328	0.00015
07	1216	815	989,824	0.00010

prevent the initial condition's influence on the analysis. The pressure was monitored at the center and along the pipe length, at 0, 0.5, 1.0, and 1.5 m.

The pressure measurements were analyzed in order to determine the slug frequency. An algorithm was implemented in the software MATLAB to calculate the PSD prominent frequency and realize a count of the pressure peaks. Also, the translational slug velocity was determined. These methods were widely described by Becker (2020).

2.4 Results and Discussion

The first results presented in this paper deal with the longitudinal mesh refinement influence on the slug frequency and onset. Figure 2 presents the results for slug frequency calculated as the normalized PSD for pressure oscillations at the pipe inlet. It can be observed that the slug frequency increases according to the longitudinal mesh refinement. Figure 3 shows the volume fraction contours at the plane normal to the gravity force and flow direction, showing a high influence of the longitudinal refinement on slug onset. Thus, it can be concluded that a large longitudinal element length postpones the onset of slug to the end of the pipe. A possible explanation for this is that large elements do not capture accurately the small oscillations that precede slug onset. Due to these preliminary analyses, it was clear that a high-quality mesh was necessary to accurately predict the slug flow, and the most longitudinally refined mesh was chosen as a base to the other meshes proposed.

Varying the global mesh refinement, a similar behavior on the slug frequency and its onset is also observed. Figure 4 shows the slug frequency calculated as the normalized PSD for pressure oscillations at the pipe inlet and Fig. 5 shows the passage of slugs in the contours of the volumetric fraction of liquid to meshes 05,

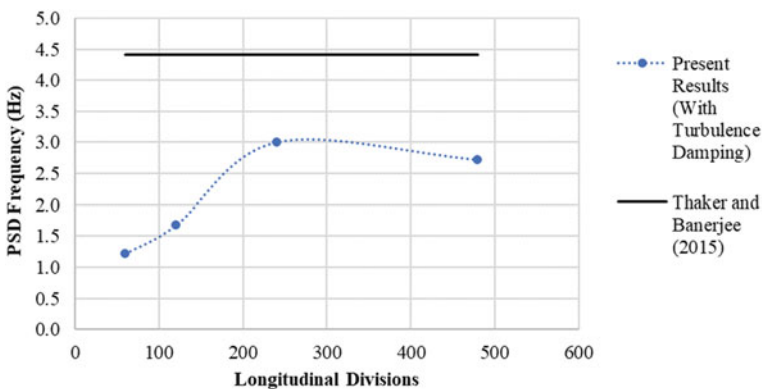


Fig. 2 Slug frequency (PSD) at the pipe inlet. Analysis considering longitudinal mesh refinement with turbulence damping

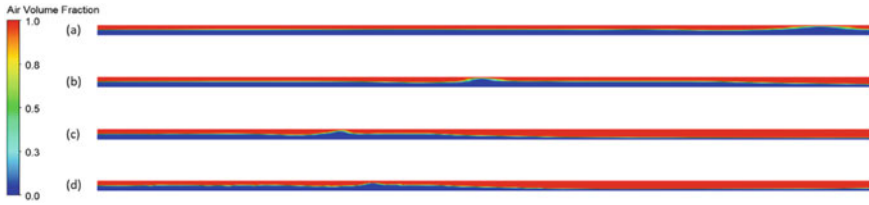


Fig. 3 Results for air volume fraction contours with turbulence damping. Comparison between the onset of slug. Analysis of the influence of longitudinal mesh refinement. **a** Mesh 01; **b** mesh 02; **c** mesh 03; **d** mesh 04

04, 06, and 07. According to mesh refinement, higher values of slug frequency were measured, but it appears that an asymptotic profile was reached, and this shows that the extra thin solution is close to being independent of the mesh. In addition, the grid index convergence was calculated, and it showed that the extra fine mesh result is close to the extrapolated mesh. The present results were compared to the empirical correlation predictions by Thaker and Banerjee (2015), and a difference of 9.3% was observed.

On the other hand, simulations were conducted using equal mesh refinement but without turbulence damping at the interface, and an interesting result is observed. Figure 6 shows the results for the counted slug frequency for simulations without turbulence damping. Results for coarse and intermediate meshes indicate that there is the formation of slugs and their frequency decreased with the refining of the mesh. However, when fine and extra fine meshes were used, slug flow was not observed, only wavy flow was observed. This observation is in opposite direction to the simulations with damping turbulence model and confirms the Lun et al. (1996) research, showing that when a poor-quality mesh is used, wiggles are generated. In this case, the numerical instabilities generated by the coarse mesh were confounded with real

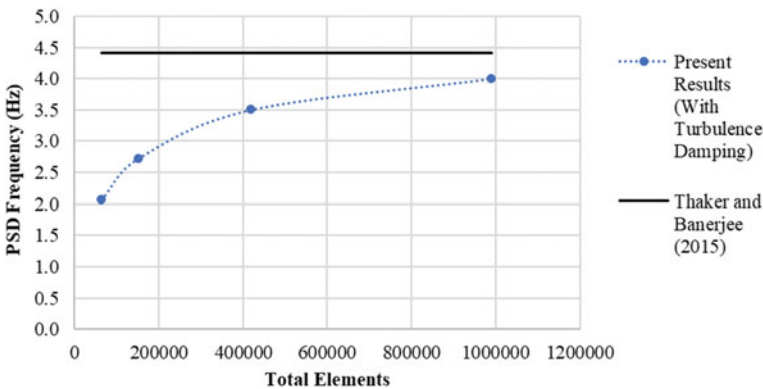


Fig. 4 Slug frequency (PSD) at the pipe inlet. Analysis for three-dimensional mesh refinement with turbulence damping



Fig. 5 Results for air volume fraction contours with turbulence damping. Comparison between the onset of slug. Analysis for tridimensional refinement influence. **a** Coarse mesh (mesh 05); **b** intermediate mesh (mesh 04); **c** fine mesh (mesh 06); **d** extra fine mesh (mesh 07)

slugs in the statistical analyses. Despite that, when a fine mesh was used, numerical instabilities decreased and, consequently, oscillations were not propagated.

Results obtained in the mesh analyses were presented in terms of static pressure oscillations at the pipe inlet. The pipe inlet analyses can represent the slug frequency as shown by Tonomura et al. (2018) with pressure measurements and visual observations. On the other hand, when other measured points along the pipe length are observed a different result is obtained, depending on the mesh refinement. Results for slug frequency along the pipe length are presented in Fig. 7, for simulations considering damping turbulence at the interface. These results showed that when a coarse and intermediate mesh were used a very similar result for slug frequency is calculated along the pipe. However, according to the mesh refinement, the slug frequency is damped along the pipe length and it corroborates with experimental observations related by Thaker and Banerjee (2015). It is important to add that this observation is valid for zero pressure at the pipe outlet, but when the pipe has a curve at the outlet, it can modify the flow characteristics (Santos 2019).

Another interesting result was obtained for the results with damping turbulence model and the finest mesh. In the last point, higher PSD frequencies are observed.

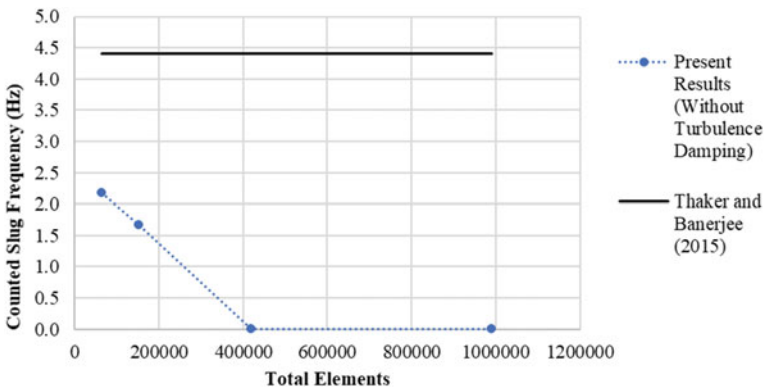


Fig. 6 Slug frequency (counted) at the pipe inlet. Analysis for three-dimensional mesh refinement without turbulence damping

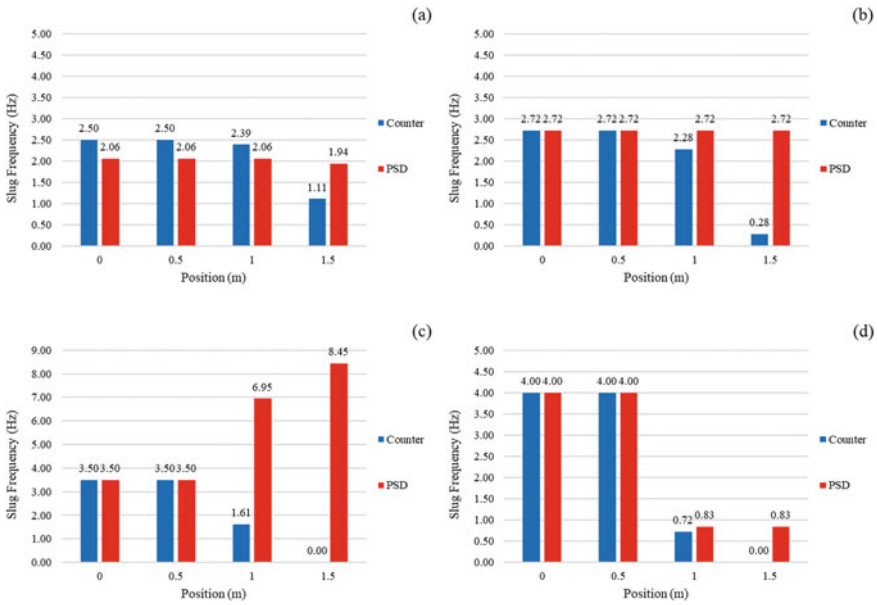


Fig. 7 Results for slug frequency at the pipe feed, simulations considering damping turbulence at the interface. Comparison between PSD prominent frequency and pressure peak counter. **a** Coarse mesh; **b** intermediate mesh; **c** fine mesh; **d** extra fine mesh

Contrary to the coarse mesh, PSD frequencies between 100 and 500 Hz are observed in the last measured point. It possibly means that a different flow pattern is occurring at the final tube region (Ujang et al. 2006). Although the VOF method used in this study is not indicated to model dispersed flow, it can be presumed that due to the mesh refinement, large bubbles and droplets are generated due to the slug break up and this explains the high-frequency oscillations. The results are shown in Fig. 8.

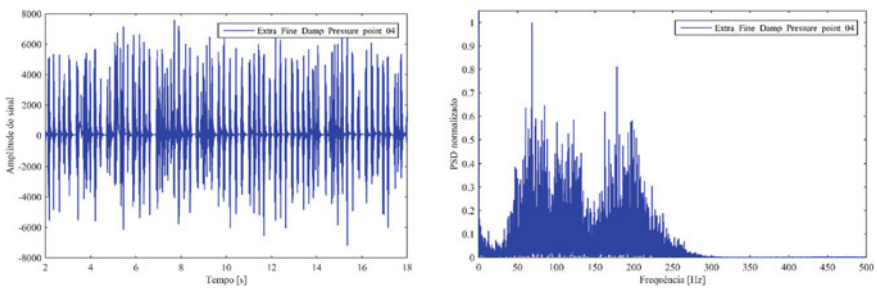


Fig. 8 Results for pressure oscillations (Pa) and PSD frequency at pipe position 1.5 m. Results for extra fine mesh

Table 2 Computational time requirement for simulations with turbulence damping

Mesh	Total elements	Number of processors	Time requirement (Days)
04	153,280	12	6.30
06	419,328	24	17.79
07	989,824	28	54.22

A comparison between the computational times required to obtain numerically 20 s of flow is presented in Table 2. The high computational time requirement for the extra fine mesh helps justify the choice of the VOF model to perform this study. After all, Akhlaghi et al. (2019) reported that the multi-fluid VOF model results in a 14 times larger computational time requirement in comparison to the VOF model, as mentioned earlier.

2.5 Conclusions

This study provided an analysis about mathematical modeling and solution methods applied to the intermittent two-phase flow patterns. It also included an overview about additional models involved in interfacial turbulence modeling. In addition, not only the spatial discretization independence was analyzed but also a validation study was conducted concerning the slug frequency. Both statistical methods used for the slug frequency analysis are shown to be useful.

Regarding mesh size uncertainty, the results showed that according to the longitudinal refinement, the frequency increased, and slugs were formed close to the pipe inlet. Moreover, high-frequency phenomena were modeled using the global mesh refinement.

An important conclusion provided by this research was that the flow was dependent on the interfacial turbulence model. The turbulence damping at the interface achieved better results, closer to the experimental observations (Thaker and Banerjee 2015). When this turbulence correction was not applied, the slug flow was not predicted.

The present results contradicted Bartosiewicz et al. (2010) ones, showing that the classical VOF method is a useful tool to predict the slug flow, even in high velocities. For this reason, the classical VOF method with turbulence damping at the interface is a viable method to be used industrially due to the lower computational cost obtained when compared with other models.

Investigating other turbulence models and the multi-fluid VOF method are suggestions for future work. Besides that, further studies should include the inlet geometry to ensure that the inlet condition does not influence the results.

Acknowledgements The authors are grateful for the financial support of PETROBRAS (research project grant number 5850.0103010.16.9), CAPES—financial code 001, and CNPq (processes 308714/2016-4).

References

- Akhlaghi M, Mohammadi V, Nouri NM, Taherkhani M, Karimi M (2019) Multi-fluid VoF model assessment to simulate the horizontal air–water intermittent flow. *Chem Eng Res Des* 152:48–59. <https://doi.org/10.1016/j.cherd.2019.09.031>
- Baker O (1953) Design of pipelines for the simultaneous flow of oil and gas. *Pet. Branch, AIME*
- Barnea D, Brauner N (1985) Holdup of the liquid slug in two phase intermittent flow. *Int J Multiph Flow* 11:43–49. [https://doi.org/10.1016/0301-9322\(85\)90004-7](https://doi.org/10.1016/0301-9322(85)90004-7)
- Barnea D, Taitel Y (1993) A model for slug length distribution in gas-liquid slug flow. *Int J Multiph Flow* 19:829–838. [https://doi.org/10.1016/0301-9322\(93\)90046-W](https://doi.org/10.1016/0301-9322(93)90046-W)
- Bartosiewicz Y, Seynhaeve J, Vallée C, Höhne T, Laviéville J (2010) Modeling free surface flows relevant to a PTS scenario: comparison between experimental data and three RANS based CFD-codes. Comments on the CFD-experiment integration and best practice guideline. *Nucl Eng Des* 240:2375–2381. <https://doi.org/10.1016/j.nucengdes.2010.04.032>
- Becker SL (2020) Estudo dos Efeitos das Propriedades Físicas do Líquido Sobre a Dinâmica do escoamento Bifásico em Duto Horizontal. Master's dissertation, University of Blumenau, Blumenau
- Cerne G, Petelin S, Tiselj I (2001) Coupling of the interface tracking and the two-fluid models for the simulation of incompressible two-phase flow. *J Comput Phys* 171:776–804. <https://doi.org/10.1006/jcph.2001.6810>
- Cook M, Behnia M (2000) Slug length prediction in near horizontal gas–liquid intermittent flow. *Chem Eng Sci* 55:2009–2018. [https://doi.org/10.1016/S0009-2509\(99\)00485-6](https://doi.org/10.1016/S0009-2509(99)00485-6)
- Fossa M, Guglielmini G, Marchitto A (2003) Intermittent flow parameters from void fraction analysis. *Flow Meas Instrum* 14:161–168. [https://doi.org/10.1016/S0955-5986\(03\)00021-9](https://doi.org/10.1016/S0955-5986(03)00021-9)
- Frederix EMA, Mathur A, Dovizio D, Geurts BJ, Komen EMJ (2018) Reynolds-averaged modeling of turbulence damping near a large-scale interface in two-phase flow. *Nucl Eng Des* 333:122–130. <https://doi.org/10.1016/j.nucengdes.2018.04.010>
- Friedemann C, Mortensen M, Nossen J (2019) Gas–liquid slug flow in a horizontal concentric annulus, a comparison of numerical simulations and experimental data. *Int J Heat Fluid Flow* 78:108437. <https://doi.org/10.1016/j.ijheatfluidflow.2019.108437>
- Gregory GA, Scott DS (1969) Correlation of liquid slug velocity and frequency in horizontal cocurrent gas–liquid slug flow. *AIChE J* 15:933–935. <https://doi.org/10.1002/aic.690150623>
- Greskovich EJ, Shrier AL (1971) Pressure drop and holdup in horizontal slug flow. *AIChE J* 17:1214–1219. <https://doi.org/10.1002/aic.690170529>
- Gueyffier D, Li J, Nadim A, Scardovelli R, Zaleski S (1999) Volume-of-fluid interface tracking with smoothed surface stress methods for three-dimensional flows. *J Comput Phys* 152:423–456. <https://doi.org/10.1006/jcph.1998.6168>
- Höhne T, Porombka P (2018) Modelling horizontal two-phase flows using generalized models. *Ann Nucl Energy* 111:311–316. <https://doi.org/10.1016/j.anucene.2017.09.018>
- Hirt CW, Nichols BD (1981) Volume of fluid (VOF) method for the dynamics of free boundaries. *J Comput Phys* 39(1):201–225. [https://doi.org/10.1016/0021-9991\(81\)90145-5](https://doi.org/10.1016/0021-9991(81)90145-5)
- Lun I, Calay RK, Holdo AE (1996) Modelling two-phase flows using CFD. *Appl Energy* 53:299–314. [https://doi.org/10.1016/0306-2619\(95\)00024-0](https://doi.org/10.1016/0306-2619(95)00024-0)
- Menter FR (1994) Two-equation eddy-viscosity turbulence models for engineering applications. *Am Inst Aeronaut Astronaut (AIAA) J* 32:1598–1605
- Nydal OJ, Pintus S, Andreussi P (1992) Statistical characterization of slug flow in horizontal pipes. *Int J Multiph Flow* 18:439–453. [https://doi.org/10.1016/0301-9322\(92\)90027-E](https://doi.org/10.1016/0301-9322(92)90027-E)
- Santos CNM (2019) Estudo Experimental e Numérico do Efeito do Duto de Saída Sobre a Dinâmica do escoamento Bifásico em Duto Horizontal. Master's dissertation, University of Blumenau, Blumenau
- Scott SL, Shoham O, Brill JP (1989) Prediction of slug length in horizontal, large-diameter pipes. *SPE Prod Eng* 4:335–340. <https://doi.org/10.2118/15103-PA>

- Shirodkar V (2015) Slug flow modelling using blended drag law and interface turbulence damping. FMFP 2015 – Paper No. 332
- Taitel Y, Dukler AE (1976) A model for predicting flow regime transitions in horizontal and near horizontal gas-liquid flow. *AIChE J* 22:47–55. <https://doi.org/10.1002/aic.690220105>
- Thaker J, Banerjee J (2015) Characterization of two-phase slug flow sub-regimes using flow visualization. *J Pet Sci Eng* 135. <https://doi.org/10.1016/j.petrol.2015.10.018>
- Tonomura O, Kobori R, Taniguchi S, Hasebe S, Matsuoka A (2018) Monitoring of two-phase slug flow in stacked multi-channel reactors based on analysis of feed pressure. *Comput Aided Chem Eng*. Elsevier Masson SAS. <https://doi.org/10.1016/B978-0-444-64241-7.50397-9>
- Ujang PM, Lawrence CJ, Hale CP, Hewitt GF (2006) Slug initiation and evolution in two-phase horizontal flow. *Int J Multiph Flow* 32:527–552. <https://doi.org/10.1016/j.ijmultiphaseflow.2005.11.005>
- Vallée C, Höhne T, Prasser HM, Sühnel T (2008) Experimental investigation and CFD simulation of horizontal stratified two-phase flow phenomena. *Nucl Eng Des* 238:637–646. <https://doi.org/10.1016/j.nucengdes.2007.02.051>
- Van Hout R, Barnea D, Shemer L (2002) Translational velocities of elongated bubbles in continuous slug flow. *Int J Multiph Flow* 28:1333–1350. [https://doi.org/10.1016/S0301-9322\(02\)00027-7](https://doi.org/10.1016/S0301-9322(02)00027-7)
- Wang X, Guo L, Zhang X (2007) An experimental study of the statistical parameters of gas-liquid two-phase slug flow in horizontal pipeline. *50:2439–2443*. <https://doi.org/10.1016/j.ijheatmasstransfer.2006.12.011>